JOURNAL OF GEOPHYSICAL RESEARCH, VOL. 100, NO. C7, PAGES 13,699–13,711, JULY 15, 1995

Bounds on the complex permittivity of sea ice

K. Golden
Department of Mathematics, University of Utah, Salt Lake City

Abstract. An analytic method for obtaining bounds on effective properties of composites is applied to the complex permittivity ϵ^* of sea ice. The sea ice is assumed to be a two-component random medium consisting of pure ice of permittivity ϵ_1 and brine of permittivity ϵ_2. The method exploits the properties of ϵ^* as an analytic function of the ratio ϵ_1/ϵ_2. Two types of bounds on ϵ^* are obtained. The first bound R_1 is a region in the complex ϵ^* plane which assumes only that the relative volume fractions p_1 and $p_2 = 1 - p_1$ of the ice and brine are known. The region R_1 is bounded by circular arcs and ϵ^* for any microgeometry with the given volume fractions must lie inside it. In addition to the volume fractions, the second bound R_2 assumes that the sea ice is statistically isotropic within the horizontal plane. The region R_2 is again bounded by circular arcs and lies inside R_1. Built into the method is a systematic way of obtaining tighter bounds on ϵ^* by incorporating information about the correlation functions of the brine inclusions. The bounding method developed here, which does not assume any specific geometry for the brine inclusions, offers an alternative to the classical mixing formula approach adopted previously in the study of sea ice. In these mixing formulas, specific assumptions are made about the inclusion geometry, which are simply not satisfied by the sea ice under many conditions. The bounds R_1 and R_2 are compared with experimental data obtained from artificially grown sea ice at the frequencies 4.8 and 9.5 GHz. Excellent agreement with the data is achieved.

1. Introduction

The remote sensing of sea ice generates many interesting technical and theoretical problems. A central question in the application of remote sensing techniques to studying sea ice is how the physical microstructure of the ice determines its scattering and effective electromagnetic properties. This question plays a fundamental role in correctly interpreting scattering data and images from sea ice. The determination of the electromagnetic properties from microstructural information is particularly interesting in the case of sea ice, which is a complex random medium consisting of pure ice with brine and air inclusions. The details of the microstructure, namely the geometry and relative volume of the inclusions, depend strongly on the temperature of the ice, the conditions under which the ice was grown, and the history of the sample under consideration, as discussed by *Weeks and Ackley* [1982]. Owing to the wide variety of possible microstructures and the high dielectric contrast of the components, it is, in general, quite difficult to accurately predict the effective complex permittivity of sea ice. Nevertheless, many models have been proposed to describe the dielectric behavior of sea ice, such as those of *Addison* [1969], *Hoekstra and Capillino* [1971], *Stogryn* [1985], *Tinga et al.* [1973], *Vant et al.* [1978], *Golden and Ackley* [1981], *Sihvola and Kong* [1988]. Typically, the sea ice is assumed to consist of a host medium (pure ice) containing spherical or ellipsoidal inclusions (brine or air). Various effective medium theories, such as the coherent potential approximation, have been used to derive "mixing formulas" for the effective permittivity ϵ^* of the system. Each formula is judged according to how well it predicts experimental data.

While mixing formulas for ϵ^* are certainly useful, their applicability to the full range of microstructures presented by sea ice is limited. For example, as sea ice warms up to around $-5°C$, the brine pockets tend to coalesce or "percolate" and form a connected matrix of brine, in which case the sea ice becomes a porous medium. This process represents an important stage in the evolution of a sea ice sheet, as it precedes the phenomenon known as "brine rejection," where some

Paper number 94JC03007.
0148-0227/95/94JC-03007$05.00

of the brine flows out of the sea ice, due to its porosity. The electromagnetic properties of the ice following the rejection are dramatically changed. Clearly the assumption that the brine (or air) component of sea ice is contained in individual ellipsoidal inclusions, is simply not satisfied when the brine forms a connected matrix. We must therefore question the validity of these mixing formulas for warm ice.

Another limitation of mixing formulas is that they provide only a precise prediction of what ϵ^* should be, given, say, a value for the brine volume and perhaps some information about the distribution of ellipsoidal orientations, as considered by *Sihvola and Kong* [1988]. They do not provide any information on the range of reasonable values for ϵ^*, which would be very useful, given that in any experiment, as one measures ϵ^* for a variety of samples, one obtains a scatter of values in the ϵ^* plane, which may or may not coincide with the precise value predicted by the mixing formula.

We remark that one of the principal motivating factors behind this work is the goal of developing practical electromagnetic methods of distinguishing sea ice types, such as first-year from multiyear ice. In typical inverse scattering algorithms, what is reconstructed from scattered electromagnetic field data is the complex permittivity which is "seen" by the wave. When the wavelength is longer than the microstructural scale, which for sea ice would correspond to frequencies of less than 10 or 20 GHz, this reconstructed permittivity will be ϵ^*, the effective permittivity. (Of course, ϵ^* itself can vary throughout any given sea ice sheet as the microstructural geometry, such as brine volume, changes through the sheet.) One of our principal goals here is to study in detail how the statistical properties of the sea ice microstructure are connected to these observed values of ϵ^*.

We also remark that another motivation for our study of sea ice is that from the point of view of the mathematical theory of composite materials, understanding the electromagnetic behavior of sea ice pushes the limits of currently available mathematical techniques. From this point of view, sea ice is an extremely interesting example of a composite material, which combines in one medium many of the challenges encountered in the development of the mathematical theory; it is a multicomponent composite, whose components have highly contrasting properties characterized by complex parameters and whose microstructure exhibits a wide range of geometries. In particular, one of the most mathematically intriguing aspects of the microstructure is the coalescing or percolation of the brine cells, which occurs around the critical temperature $T_c \approx -5°\mathrm{C}$, and results in a microstructural transition from separated brine pockets to a connected brine matrix. The influence of the connectedness properties of composite microstructures on bulk electromagnetic behavior has been a topic of considerable recent mathematical interest. For example, see *Kozlov* [1989], *Golden* [1990], *Golden* [1992], *Golden* [1994], *Berlyand and Golden* [1994], *Bruno* [1991] and K. Golden [Statistical mechanics of conducting phase transitions, submitted to J. Math. Phys., 1995]. It is interesting to note in this context that the connectedness properties of a particular component dominate the behavior of many technologically important materials, including doped semiconductors, porous media (e.g., sandstones), piezocomposites, thermistors, solid rocket propellants, and cermets.

2. Description of Theory and Methods

Owing to the above limitations in the mixing formula approach which are caused by the wide variety of relevant sea ice microstructures, we begin here a new approach to studying the effective complex permittivity ϵ^* of sea ice by obtaining bounds on ϵ^* in the complex plane. As a first step in the development of this approach, we consider the sea ice to be a two-component random medium consisting of pure ice of complex permittivity ϵ_1 in the volume fraction p_1 and brine of complex permittivity ϵ_2 in the volume fraction $p_2 = 1 - p_1$. In this paper we will neglect the effects of air inclusions, which is a reasonable assumption in many situations, such as for first year ice which has not yet undergone brine rejection, where air can replace much of the brine. To obtain the bounds, we apply a method introduced independently by *Bergman* [1978] and *Milton* [1979] which exploits the properties of ϵ^* as an analytic function of the ratio ϵ_1/ϵ_2. The method was developed further and applied in various settings by both Bergman and Milton, and the complex bounds used here were obtained independently by *Milton* [1981] and *Bergman* [1980]. A mathematical formulation of the method was given by *Golden and Papanicolaou* [1983] and some of its implications were explored by *Milton and Golden* [1985].

The key step in this formulation is establishing an integral representation for ϵ^*, which is then used to obtain the bounds. As in the case of typical mixing formulas, the bounds are derived in the quasi-static limit, so that they are valid when the wavelength is long compared to the scale of the inhomogeneities.

We now describe the bounds more precisely. For the simplest bound it is assumed that only ϵ_1, ϵ_2, p_1, and p_2 are known. The bound consists of a lens-shaped region in the complex ϵ^* plane in which the values of ϵ^* for all possible mixtures of the two materials in the given volume fractions must lie. For the case of sea ice, where there is a wide variety of possible microstructures, the bound is valid for all of them, given only the brine volume. Built into the method, though, is a systematic way of obtaining tighter bounds on ϵ^* if one knows further statistical information about the geometry beyond simply the volume fractions. More precisely, there is a hierarchy of increasingly tighter bounds, where the nth order bound depends on knowledge of the n–point cor-

relation function of the mixture. The bounds described above are first order and depend only on one–point correlation or volume fraction information. For the case of second-order bounds it turns out that if the material is statistically isotropic, i.e., if ϵ^* does not depend on the direction of polarization of the electric field, then one can obtain the bounds without any direct knowledge of the two–point correlation function.

In the present work we apply the first order and isotropic second order bounds to sea ice with given salinities and temperatures. These bounds are compared with the experimental data of *Arcone et al.* [1986] for artificially grown sea ice at 4.8 and 9.5 GHz. Given a sample of sea ice at temperature T and of salinity S, we estimate the brine volume p_2 using the equation of *Frankenstein and Garner* [1967]. Then for each frequency, 4.8 and 9.5 GHz, and for a given temperature T, we find the complex permittivity of the brine ϵ_2 using the calculations of *Stogryn and Desargant* [1985]. In general, we obtain excellent agreement with the experimental data. Small discrepancies between the bounds and the real data are inevitable, though, and may be explained with uncertainties in the brine volumes, the unaccounted for presence of air, or scattering effects when the wavelength is larger but comparable to the typical brine length scale.

3. Bounds on the Effective Permittivity

We now present the bounds on ϵ^* discussed above. In this section we first formulate the effective permittivity problem, briefly describe the method for obtaining the bounds, which is called the analytic continuation method, and then state the bounds. A more detailed summary of the method is given in the appendix. We also refer the interested reader to *Golden and Papanicolaou* [1983], *Golden* [1986] and *Bergman* [1982] for more detail.

Let us begin by formulating the effective complex permittivity problem for a two-component random medium in all of $\mathbb{R}^d$, d-dimensional Euclidean space, with translation invariant statistics. Formulating the problem in this way is for mathematical simplicity but is analogous to assuming that the brine statistics are the same throughout a given sample of sea ice and that the sample is large compared to the typical brine length scale, which is reasonable for comparison with data taken for samples by *Arcone et al.* [1986]. For real sea ice the brine statistics and structure will change with depth and might differ from floe to floe. However, for a relatively small depth interval of, say, 10 cm, and in any given floe the assumption should be reasonably well satisfied. Now let $\epsilon(\mathbf{x},\omega)$ be a (spatially) stationary random field in $\mathbf{x} \in \mathbb{R}^d$ and $\omega \in \Omega$, where Ω is the set of all realizations of our random medium. (We are dealing here with an ensemble Ω of random media, indexed by the parameter ω, which represents one particular realization and not frequency.) For a two–component medium with component permittivities ϵ_1 (ice) and ϵ_2 (brine) we write

$$\epsilon(\mathbf{x},\omega) = \epsilon_1\chi_1(\mathbf{x},\omega) + \epsilon_2\chi_2(\mathbf{x},\omega), \tag{1}$$

where χ_j is the characteristic function of medium $j = 1,2$, which equals one for all realizations $\omega \in \Omega$ having medium j at $\mathbf{x}$, and equals zero otherwise. Let $\mathbf{E}(\mathbf{x},\omega)$ and $\mathbf{D}(\mathbf{x},\omega)$ be the stationary random electric and displacement fields, respectively, satisfying

$$\mathbf{D}(\mathbf{x},\omega) = \epsilon(\mathbf{x},\omega)\mathbf{E}(\mathbf{x},\omega) \tag{2}$$

$$\nabla \cdot \mathbf{D}(\mathbf{x},\omega) = 0 \tag{3}$$

$$\nabla \times \mathbf{E}(\mathbf{x},\omega) = 0 \tag{4}$$

$$< \mathbf{E}(\mathbf{x},\omega) >= \mathbf{e}_k, \tag{5}$$

where $\mathbf{e}_k$ is a unit vector in the kth direction, for some $k = 1,\ldots,d$. In (5), angle brackets mean ensemble average over Ω or spatial average over all of $\mathbb{R}^d$.

In view of the local constitutive law (2) we define the effective complex dielectric tensor $\boldsymbol{\epsilon}^*$ via

$$< \mathbf{D} > \;=\; \boldsymbol{\epsilon}^* < \mathbf{E} >, \quad k = 1,\ldots,d, \tag{6}$$

or,

$$\epsilon^*_{ik} \;=\; < D_i >, \quad i,k = 1,\ldots d, \tag{7}$$

where the right side of (7) depends on k via (2) and (5). For simplicity we focus on one diagonal coefficient $\epsilon^* = \epsilon^*_{kk}$. Noting that through the homogeneity property $\epsilon^*(\lambda\epsilon_1,\lambda\epsilon_2) = \lambda\epsilon^*(\epsilon_1,\epsilon_2)$, ϵ^* depends only on the ratio $h = \epsilon_1/\epsilon_2$, we may divide (7) by ϵ_2 and define

$$m(h) = \frac{\epsilon^*}{\epsilon_2} = < (h\chi_1 + \chi_2)E_k >, \quad h = \frac{\epsilon_1}{\epsilon_2}. \tag{8}$$

The two main properties of $m(h)$ are that it is analytic off the interval $(-\infty, 0]$ in the h plane and that it maps the upper half plane to the upper half plane, i.e. ,

$$Im(m(h)) > 0, \qquad Im(h) > 0, \tag{9}$$

where Im denotes imaginary part. Such functions which are analytic off some segment of the real axis and obey (9) are called Herglotz functions.

As mentioned in section 2, the key step in the analytic continuation method is obtaining an integral representation for ϵ^*. For this purpose it is more convenient to look at the function

$$F(s) = 1 - m(h), \quad s = 1/(1-h), \tag{10}$$

which is analytic off $[0,1]$ in the s plane. It was then proven by *Golden and Papanicolaou* [1983] that $F(s)$ has the following representation

$$F(s) = \int_0^1 \frac{d\mu(z)}{s-z}, \tag{11}$$

where μ is a positive measure on $[0,1]$. (Very loosely

speaking, we may think of $d\mu(z)$ as $g(z)dz$, for some density $g(z)$ which is allowed to have "δ function" components.) One of the most important features of (11) is that it separates the parameter information in $s = 1/(1-\epsilon_1/\epsilon_2)$ from information about the geometry of the mixture, which is all contained in μ, through dependence on χ_1. In fact, statistical information about the geometry is input into (11) via the moments of μ,

$$\mu_n = \int_0^1 z^n d\mu(z). \tag{12}$$

This input is obtained by equating an expansion of (11) in powers of $1/s$, the coefficients of which are the moments μ_n, to a corresponding perturbation expansion around a homogeneous medium ($s = \infty$ or $\epsilon_1 = \epsilon_2$) of another representation for $F(s)$ involving a resolvent formula for $\mathbf{E}$. This procedure, which is described in the appendix, yields

$$\mu_0 = p_1, \tag{13}$$

if only the volume fractions are known, and

$$\mu_1 = \frac{p_1 p_2}{d} \tag{14}$$

if the material is statistically isotropic, where d is the dimension of the system as in 6 and (7). In general, knowledge of the $(n+1)$-point correlation function of the medium allows calculation of μ_n (in principle).

Bounds on ϵ^* or $F(s)$ are obtained by fixing s in (11), varying over admissible measures μ (or admissible geometries), such as those that satisfy only (13), and finding the corresponding range of values of $F(s)$. This procedure is described in the appendix. We now give formulas for the boundaries of these regions. In addition to the first- and second-order bounds described in the Introduction, there are zeroth order bounds which assume no knowledge of the geometry, not even the volume fractions. They exploit only the conditions that $0 \le \mu_0 \le 1$ and $F(s=1) \le 1$. In the F plane, let R_0 be the region containing the range of values of $F(s)$. Then R_0 is bounded by a circular arc $C(\alpha)$ and a line segment $L(\alpha)$,

$$C(\alpha) = \frac{\alpha}{s-(1-\alpha)}, \quad L(\alpha) = \frac{\alpha}{s}, \quad 0 \le \alpha \le 1. \tag{15}$$

The arc $C(\alpha)$ is circular because as a function of α, $C(\alpha)$ is a fractional linear transformation of α, which maps the class of circles and lines to itself. When s is complex, then the line segment $[0,1]$ in the α plane gets mapped to an arc of a circle. If we transform R_0 to the ϵ^* plane, then its vertices are ϵ_1 and ϵ_2, $L(\alpha)$ gets transformed to the line segment

$$L^*(\alpha) = \alpha\epsilon_1 + (1-\alpha)\epsilon_2, \quad 0 \le \alpha \le 1, \tag{16}$$

and $C(\alpha)$ gets transformed to the circular arc

$$C^*(\alpha) = \left(\frac{\alpha}{\epsilon_1} + \frac{1-\alpha}{\epsilon_2}\right)^{-1}, \qquad 0 \le \alpha \le 1, \tag{17}$$

so that α plays the role of p_1, the volume fraction of medium 1. In fact, the expressions in (16) and (17) are simply the complex permittivities of laminates (or layers) of ϵ_1 and ϵ_2 in the relative volume fractions α and $1-\alpha$ with the applied field parallel and perpendicular, respectively, to the lamination direction. The arc and line segment are parameterized by the relative volume fraction α of ϵ_1. Because there are actual geometries (laminates) which attain these complex bounds, the bounds are said to be optimal, in other words, with no assumptions at all about the geometry, these are the best bounds one can obtain. For real parameters with $\epsilon_1 \le \epsilon_2$, R_0 collapses to the interval

$$\epsilon_1 \le \epsilon^* \le \epsilon_2. \tag{18}$$

If the volume fractions p_1 and $p_2 = 1-p_1$ are known, then (13) must be satisfied. Let R_1 be the corresponding region, which is bounded by circular arcs. In the F plane one of these arcs is parameterized by

$$C_1(z) = \frac{p_1}{s-z}, \qquad 0 \le z \le p_2, \tag{19}$$

where z is a real parameter and $C(z)$ is fractional linear in z, like $C(\alpha)$ above. To exhibit the other arc, it is convenient to consider the auxiliary function

$$E(s) = 1 - \frac{\epsilon_1}{\epsilon^*} = \frac{1-sF(s)}{s[1-F(s)]}, \tag{20}$$

which is a Herglotz function like $F(s)$, analytic off $[0,1]$. Then in the E plane, we can parameterize the other circular boundary of R_1 by

$$\hat{C}_1(z) = \frac{p_2}{s-z}, \qquad 0 \le z \le p_1. \tag{21}$$

In the ϵ^* plane, R_1 has vertices $p_1\epsilon_1 + p_2\epsilon_2$ and $(p_1/\epsilon_1 + p_2/\epsilon_2)^{-1}$ and is bounded by the arcs

$$C_1^*(\beta) = \epsilon_2 + p_1 \Big/ \left(\frac{1}{\epsilon_1-\epsilon_2} + \frac{\beta p_2}{\epsilon_2}\right), \quad 0 \le \beta \le 1, \tag{22}$$

$$\hat{C}_1^*(\beta) = \epsilon_1 + p_2 \Big/ \left(\frac{1}{\epsilon_2-\epsilon_1} + \frac{\beta p_1}{\epsilon_1}\right), \quad 0 \le \beta \le 1, \tag{23}$$

where β is a real parameter and $C_1^*(\beta)$ and $\hat{C}_1^*(\beta)$ are again fractional linear in β. Again, these bounds are optimal and are attained by a number of geometries, including coated elliptical cylinders considered by *Milton* [1981]. When ϵ_1 and ϵ_2 are real, R_1 collapses to the interval

$$(p_1/\epsilon_1 + p_2/\epsilon_2)^{-1} \le \epsilon^* \le p_1\epsilon_1 + p_2\epsilon_2, \tag{24}$$

which are the classical arithmetic and harmonic mean bounds.

If the material is further assumed to be statistically isotropic, i.e., $\epsilon^*_{ik} = \epsilon^* \delta_{ik}$, then (14) must be satisfied as well. The corresponding region R_2, again, has circular arcs for boundaries. In the F plane one of these arcs is parameterized by

$$C_2(z) = \frac{p_1(s-z)}{s(s-z-p_1/d)}, \quad 0 \le z \le (d-1)/d. \quad (25)$$

In the E plane the other arc is parameterized by

$$\hat{C}_2(z) = \frac{p_2(s-z)}{s[s-z-p_1(d-1)/d]}, \quad 0 \le z \le 1/d. \quad (26)$$

When ϵ_1 and ϵ_2 are real with $\epsilon_1 \le \epsilon_2$, R_2 collapses to the interval

$$\epsilon_1 + p_2 \Big/ \left(\frac{1}{\epsilon_2 - \epsilon_1} + \frac{p_1}{d\epsilon_1}\right) \le \epsilon^* \le \epsilon_2 + p_1 \Big/ \left(\frac{1}{\epsilon_1 - \epsilon_2} + \frac{p_2}{d\epsilon_2}\right), \quad (27)$$

which are the famous bounds of *Hashin and Shtrikman* [1962]. The real bounds in (27) are attainable by coated sphere geometries, but the complex arcs (25) and (26) are not generally attainable, as noted by *Milton* [1981] and *Bergman* [1982].

4. Comparison With Experimental Data

In this section we consider plots of the bounds R_0, R_1, and R_2 and compare them with the experimental data of *Arcone et al.* [1986]. For any given sample of sea ice of salinity S and temperature T the brine volume p_2 may be estimated using the equation of *Frankenstein and Garner* [1967],

$$p_2 = S\left(\frac{49.185}{T} + 0.532\right). \quad (28)$$

To determine ϵ_2, the complex permittivity of the brine, we use the empirically determined formulas of *Stogryn and Desargant* [1985], which are based on a Debye-type relaxation equation,

$$\epsilon_2 = \epsilon_\infty + \frac{\epsilon_s - \epsilon_\infty}{1 - i2\pi f\tau} + i\frac{\sigma}{2\pi\epsilon_0 f}, \quad (29)$$

which has only one resonance, ignoring a possible spread in relaxation times. In (29), ϵ_s and ϵ_∞ are the limiting static and high frequency values of the real part of $\epsilon_2, Re(\epsilon_2)$, τ is the relaxation time, f is the frequency, σ is the ionic conductivity of the dissolved salts, ϵ_0 is the permittivity of free space, and $i = (-1)^{1/2}$. The ionic conductivity is assumed to be independent of frequency. Then ϵ_2 for brine in equilibrium with sea ice is determined by the four real parameters $\epsilon_\infty, \epsilon_s, \tau$, and σ, each of which depends only on temperature, and all were found experimentally. Compared to the brine, the complex permittivity of the pure ice ϵ_1 is basically independent of temperature and frequency, as found by *Mätzler and Wegmüller* [1987], and we take $\epsilon_1 = 3.15 + i0.002$.

In Figure 1 we plot the bound R_0 with R_1 contained inside, with the frequency, S, T, and p_2 values shown. Clearly, knowing the brine volume (R_1) yields a tremendous improvement over the R_0 bound, which only assumes knowledge of the values of ϵ_1 and ϵ_2. In Figure 2 we have plotted two different regions R_1 for the same sample of sea ice with $S = 5^0/_{00}$, to show how changing the temperature shifts the region in the ϵ^* plane. Alternatively, we can view Figure 2 as showing how changing the brine volume can dramatically affect the location and size of R_1. In Figure 3 we have plotted the smaller R_1 with $T = -11°C$ from Figure 2 with R_2 inside of it. For the calculation of R_2 here and in subsequent figures, whose boundaries are given by (25) and (26), we have used $d = 2$, since as the wave propagates vertically down through a slab which is not too thick, the properties are reasonably uniform in this direction. In this case the electric field only has components within the horizontal plane, so that the system is effectively two-dimensional. The assumption of isotropy in this configuration, which is the configuration used by *Arcone et al.* [1986], is then an assumption about isotropy within the horizontal plane, which is a topic considered by *Cherepanov* [1971], *Kovacs and Morey* [1978], *Weeks and Gow* [1980] and *Golden and Ackley* [1981]. (We remark that since the scales on the $Re(\epsilon^*)$ and $Im(\epsilon^*)$ axes are not the same, the circular arcs which form the boundaries of the regions may not necessarily appear circular.)

In Figures 4a, 4b, and 4c we begin the comparison of our bounds with the measured values of ϵ^* for artificially grown sea ice of *Arcone et al.* [1986]. The data points in Figure 4a were taken from *Arcone et al.* [1986], Figure 8. They represent a range of p_2 values from 0.031 to 0.041, and salinity values from $3.8^0/_{00}$ to $4.4^0/_{00}$. To construct the bound, we have chosen the midpoint values of $p_2 = 0.036$ and $S = 4.1\ ^0/_{00}$, and then inverted (28) to obtain $T = -6°C$. The data points in Figure 4b range in p_2 values from 0.018 to 0.023, with the same salinity range as in Figure 4a, and we obtain the bound through the same midpoint procedure. In Figure 4c, the data have been taken from the 85-4 slab measurements of *Arcone et al.* [1986], Figure 17, with a range in temperature from $-12.5°C$ to $-15.5°C$, so that we choose the midpoint $T = -14°C$, with $S = 2.4^0/_{00}$, to construct the bound. We chose this particular slab because there was little difference between the measured salinity before and after the experiments were done, so that we were fairly confident that the p_2 value given by (28) would be representative of what was in the sample. By comparison of the data with R_2, there appears to be some evidence of a small degree of anisotropy, which agrees with what was found directly by *Arcone et al.* [1986]. However, these dis-

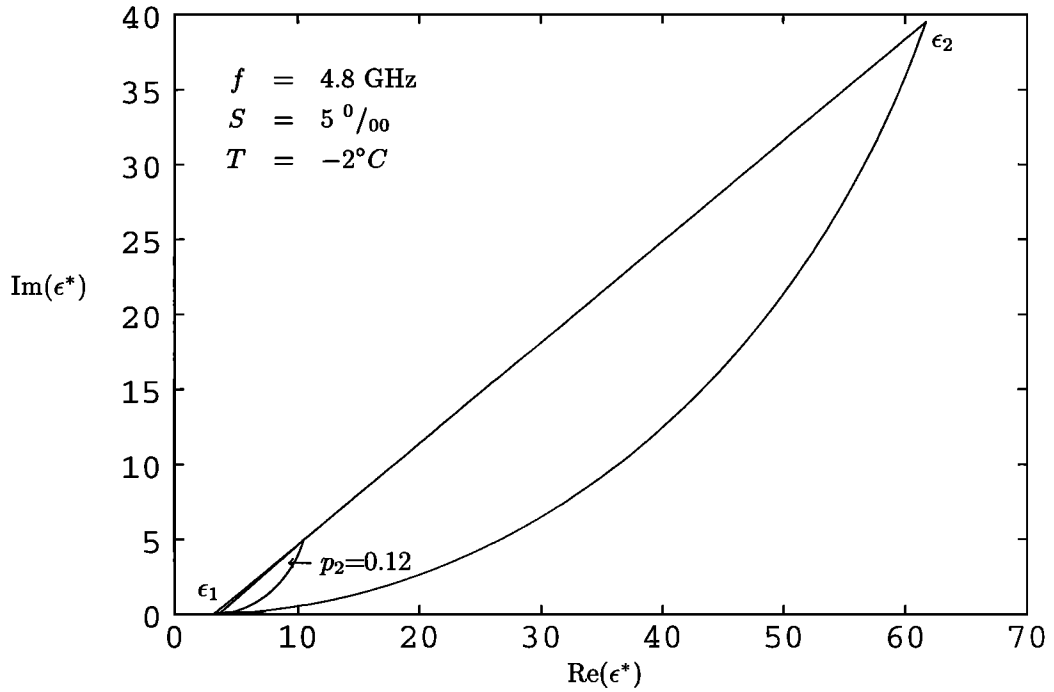

Figure 1. Bounds on complex permittivity ϵ^* for sea ice. The large region R_0 assumes nothing about the microstructure. The small region R_1 inside assumes a brine volume of $p_2 = 0.12$; f is frequency, S is salinity, and T is temperature.

crepancies may also be accounted for by uncertainties in the brine volume, which is discussed below.

Finally, Figures 5a, 5b, 6a, and 6b were created to be able to directly compare with *Arcone et al.* [1986, Figures 16 and 17], in which the real and imaginary parts of ϵ^* are plotted separately as a function of temperature. The data shown in our figures are a representative set of the data from slabs 85-1, 85-2, and 85-3. These three slabs were chosen because their salinity values (before the experiment) were all close to each other, with $S = 4.8, 5.5$ and 5.4 $^0/_{00}$, respectively. *Arcone et al.* [1986, Figures 16 and 17] plot data for ice which is

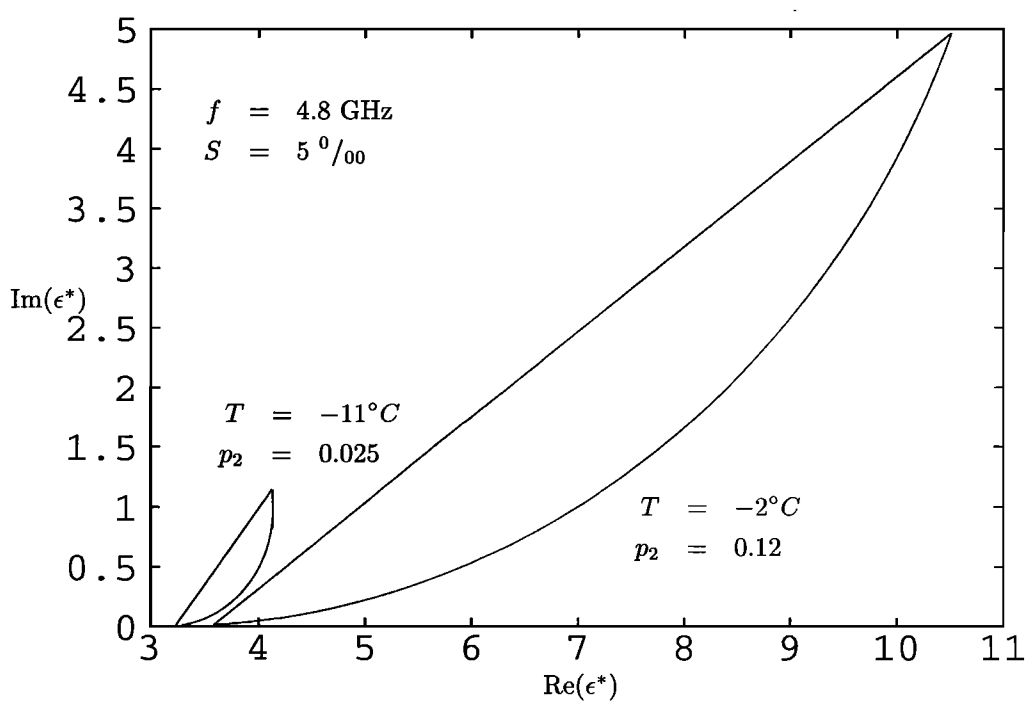

Figure 2. Bounds on ϵ^* for sea ice with different brine volumes p_2 or different temperatures T.

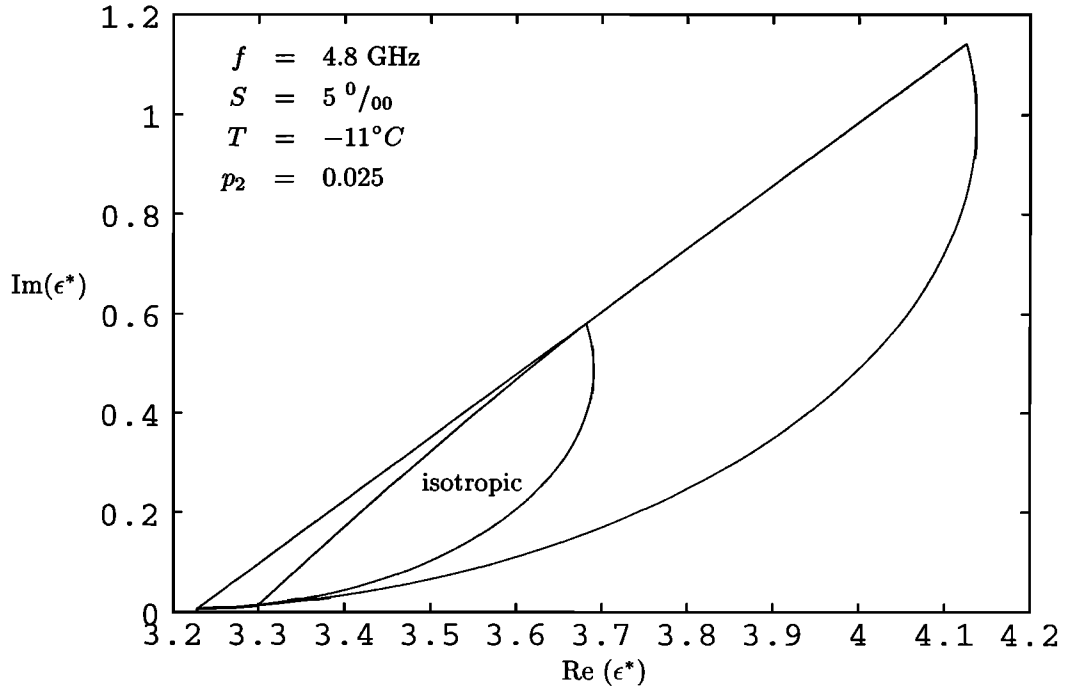

Figure 3. Bounds on ϵ^* for given brine volume (outer bound R_1) and assuming isotropy within the horizontal plane (inner bound R_2).

warmed and subsequently cooled down. We only used the "warming" data, as once the ice has been warmed above −5°C, brine leaks out and air replaces some of the brine, which is reflected in the "cooling" data. For any given value of T, to create the upper and lower bounds shown in our figures, we first computed the R_2 bounds for that value of T and with $S = 5\ ^0/_{00}$. For a given value of T, the R_2 bound gives a maximum and minimum value for both $Re(\epsilon^*)$ and $Im(\epsilon^*)$ which corresponds to the coordinates of the vertices of R_2. The upper and lower bounds for any given T shown in Figure 5a, for example, correspond to these maxi-

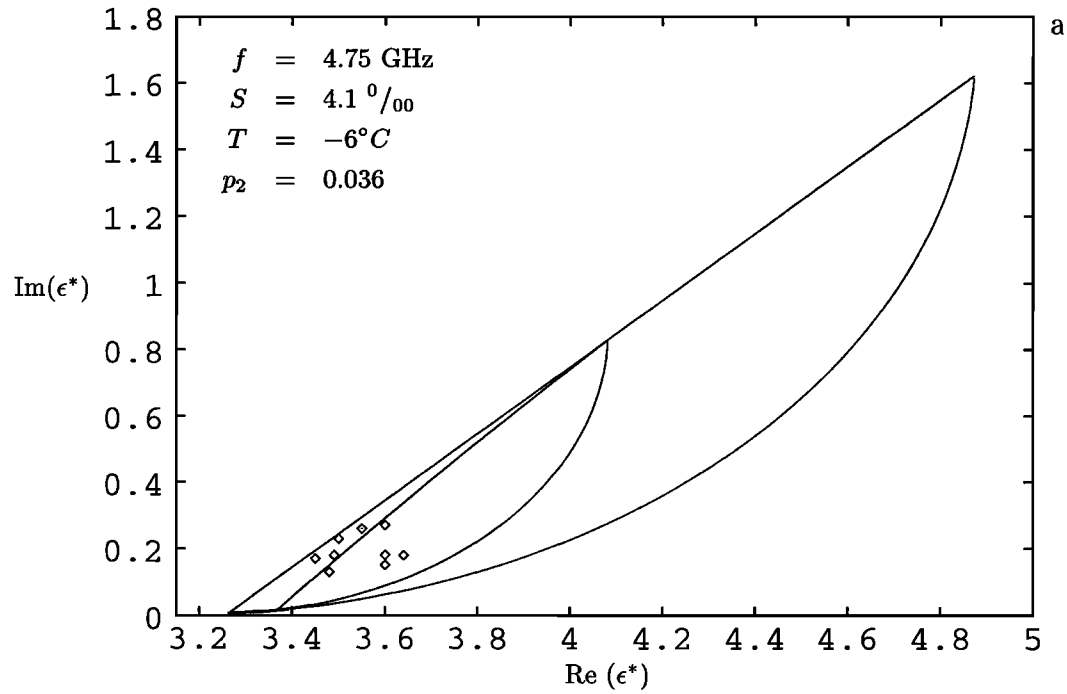

Figure 4a. Comparison of experimental data on ϵ^* with R_1 for given brine volume p_2 and with bound R_2 which assumes isotropy as well.

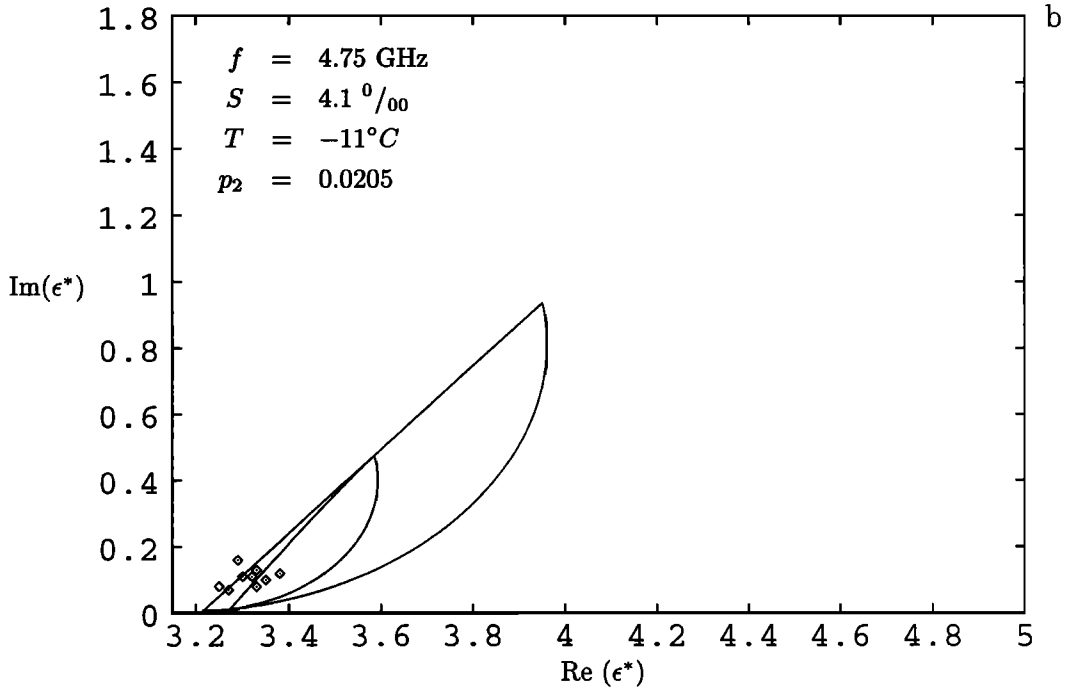

Figure 4b. Same as Figure 4a, except for temperature of −11°C and p_2 of 0.0205.

mum and minimum values of $Re(\epsilon^*)$ obtained from the vertices of R_2. Note that by considering $Re(\epsilon^*)$ and $Im(\epsilon^*)$ separately, it is easier for data points to lie inside the bounds, compared with plotting the points in the complex plane. More precisely, points which lie inside the bounds represented in Figures 5a, 5b, 6a, and 6b, if plotted in the complex ϵ^* plane, would only be required to lie in the corresponding rectangle (with sides parallel to the axes) with two vertices matching the two vertices of R_2. Because of this added flexibility through plotting $Re(\epsilon^*)$ and $Im(\epsilon^*)$ separately, we found that we could obtain good fit with the data by using R_2 instead of R_1. We remark that the assumption of isotropy in the horizontal plane, which is implicit in constructing R_2, is fairly reasonable, as seen in the previous figures. Furthermore, since the sea ice was artifi-

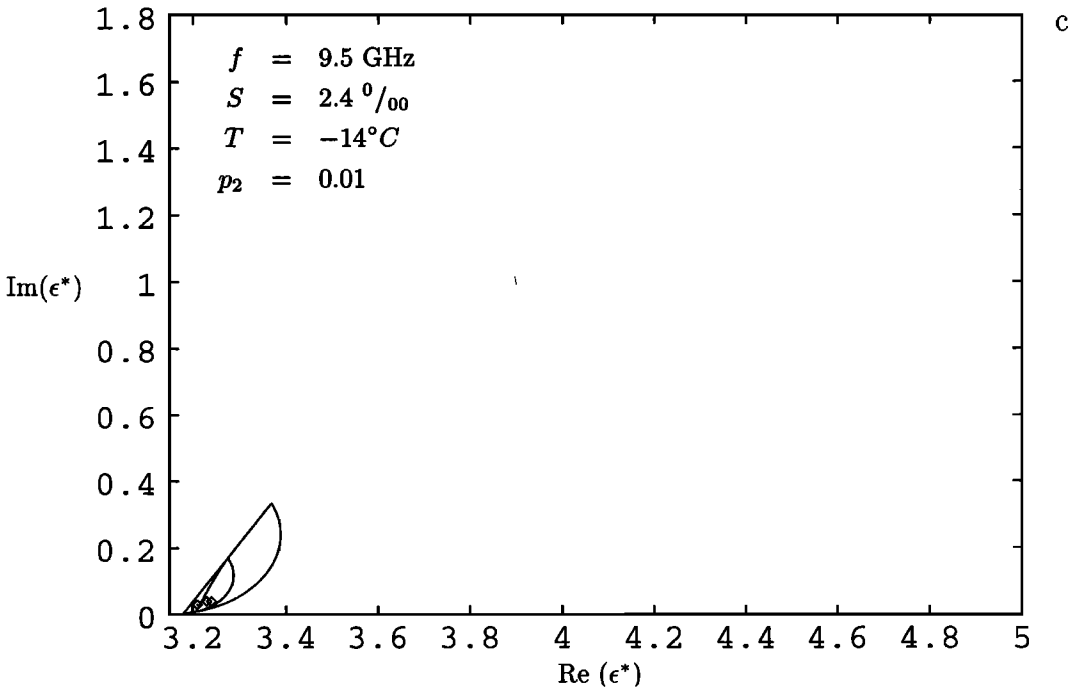

Figure 4c. Same as Figure 4a, except for frequency of 9.5 GHz, salinity of $2.4^0/_{00}$, temperature of −14°C, and p_2 of 0.0l.

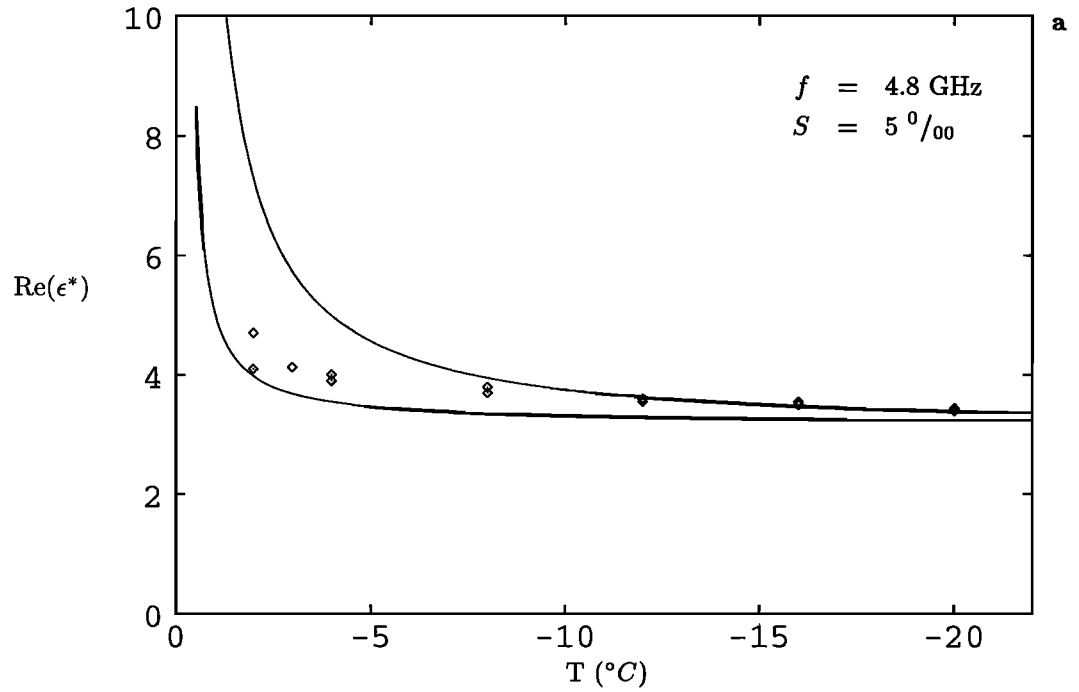

Figure 5a. Comparison of experimental data on ϵ^* with upper and lower bounds on $Re(\epsilon^*)$ obtained from R_2, as a function of temperature, at 4.8 GHz.

cially grown in an outdoor pool, where there is no well-developed, long-term current direction (which is usually present when the c axis orientation of sea ice is highly anisotropic, as studied by *Cherepanov* [1971], *Weeks and Gow* [1980] and *Golden and Ackley* [1981]), we should not expect marked anisotropy in the data from *Arcone et al.* [1986].

5. Discussion

In comparing our bounds with the data of *Arcone et al.* [1986], we have found that perhaps the single most important quantity which determines the dielectric properties of sea ice is the brine volume p_2, and the regions R_1 and R_2 are very sensitive to this value. Un-

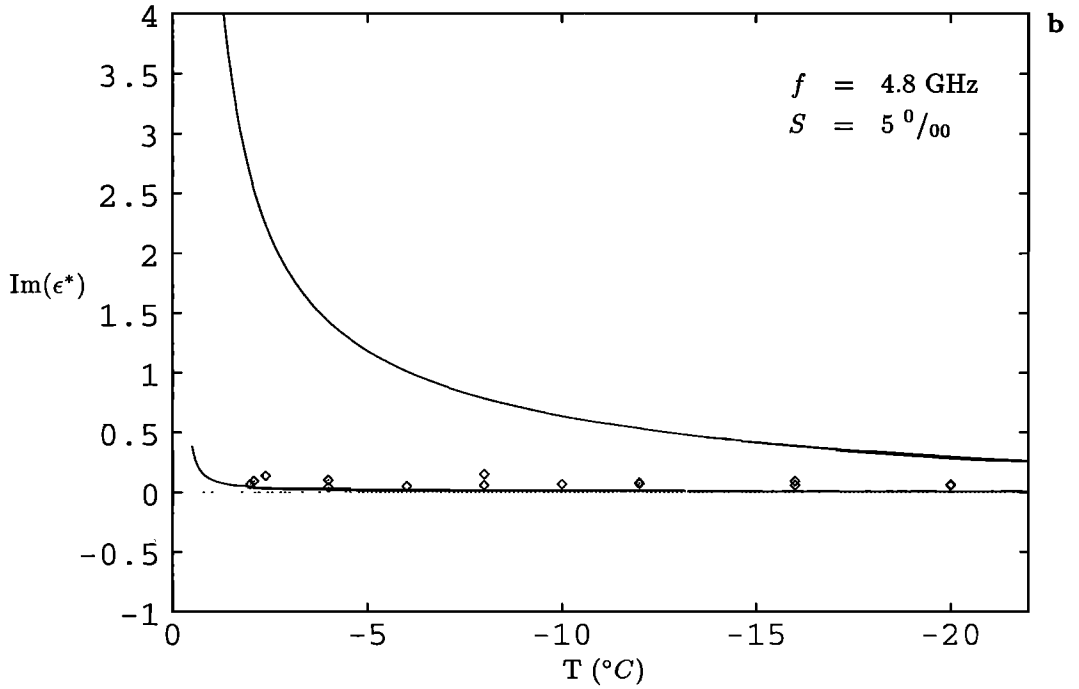

Figure 5b. Comparison of experimental data on ϵ^* with upper and lower bounds on $Im(\epsilon^*)$ obtained from R_2, as a function of temperature, at 4.8 GHz.

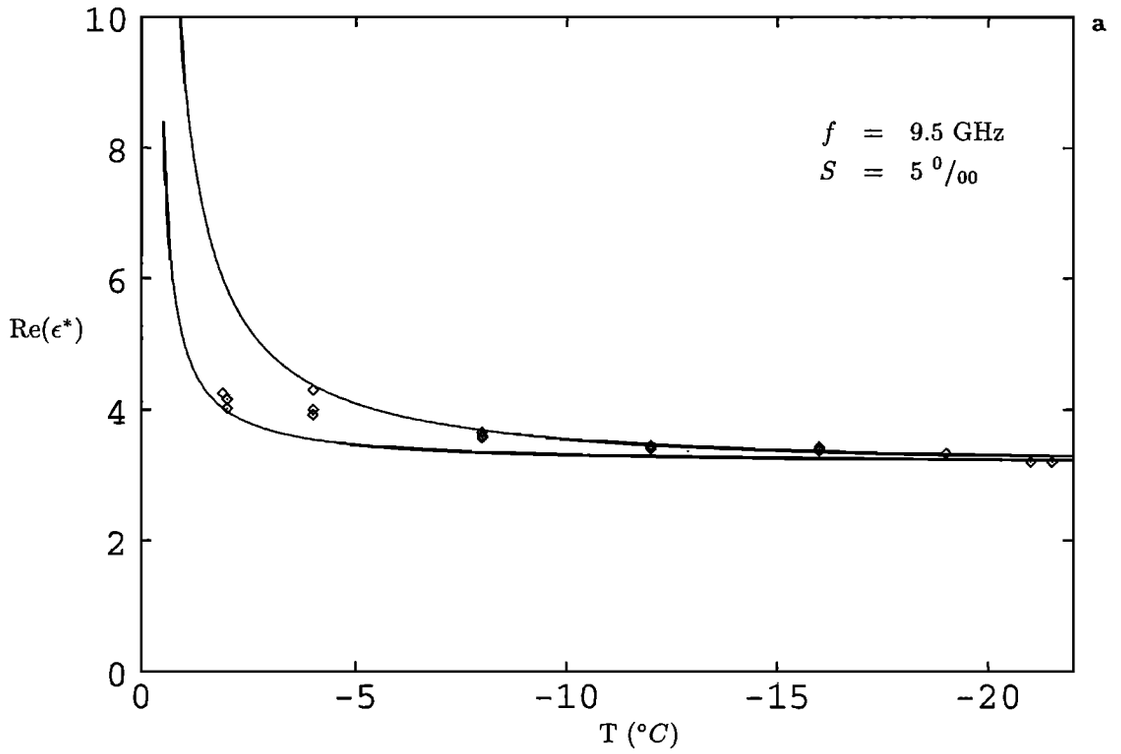

Figure 6a. Comparison of experimental data on ϵ^* with upper and lower bounds on $Re(\epsilon^*)$ obtained from R_2, as a function of temperature, at 9.5 GHz.

fortunately, the brine volume is quite difficult to measure experimentally. In comparing our bounds with the data, it appeared that the largest discrepancies occurred when there was the most uncertainty in the calculated value of the brine volume. As Arcone et. al. note, brine was leaking out of the slabs of sea ice until their temperature dropped below −24°C, and resumed again with T between −5° and −6°C. Even though the leaked brine was collected so that accurate salinity measurements could be made, under such circumstances the equation of *Frankenstein and Garner* [1967], which is based on theoretical considerations, cannot be expected to provide a very accurate prediction of the actual brine volume in the sample. In fact, we noted that adjusting the brine volume in the bound R_1 could usually capture any scatter of data points associated with a particular S, T pair. This observation leads one to suspect that the brine volume of a given sample of sea ice could be deduced by measuring ϵ^* at a number of different frequencies and checking which brine volume yields the best correspondence between the bounds and the data.

As mentioned in section 2, the bounds are derived in the quasi–static or infinite wavelength limit and are valid when the wavelength λ is large compared with the typical brine length scale β, which is of the order of millimeters. When λ becomes comparable to β, we might expect that scattering effects become more significant. In this case we would expect that measured values of $Im(\epsilon^*)$ should be higher than those predicted by the bounds due to scattering losses. For the current frequencies of 4.8 and 9.5 GHz we have found no evidence of any systematic offset of the experimental values when compared with the bounds. We conclude then that at these frequencies, scattering losses are minimal. In current work with S. Ackley and V. Lytle, we are comparing the quasi-static bounds with higher–frequency data, over a range of 26.5–40.0 GHz, where the validity of the quasi-static assumption is uncertain. This work will be reported elsewhere.

Finally, as mentioned in section 4, we did not use the "cooling" data of *Arcone et al.* [1986], as air has replaced some of the brine. The effect this has on ϵ^* is that it apparently lowers the measured values of both $Re(\epsilon^*)$ and $Im(\epsilon^*)$. In order to obtain bounds to model this situation, as well as multiyear ice which generally has more air volume than does first year ice, we must consider the sea ice to be a three-component random medium consisting of pure ice, brine, and air. However, the mathematical theory of bounding ϵ^* for three or more components is quite a bit more involved than for two, and involves the theory of several complex variables in which there arise new mathematical phenomena not encountered with functions of a single complex variable. In fact, the general theory of complex bounds was restricted to two components until the work of *Golden and Papanicolaou* [1985], and the first set of comprehensive bounds on ϵ^* in the multicomponent case was found by *Golden* [1986]. Subsequently, *Milton* [1987a,b] improved Golden's bounds and significantly extended the bounding theory. In subsequent work we would like to

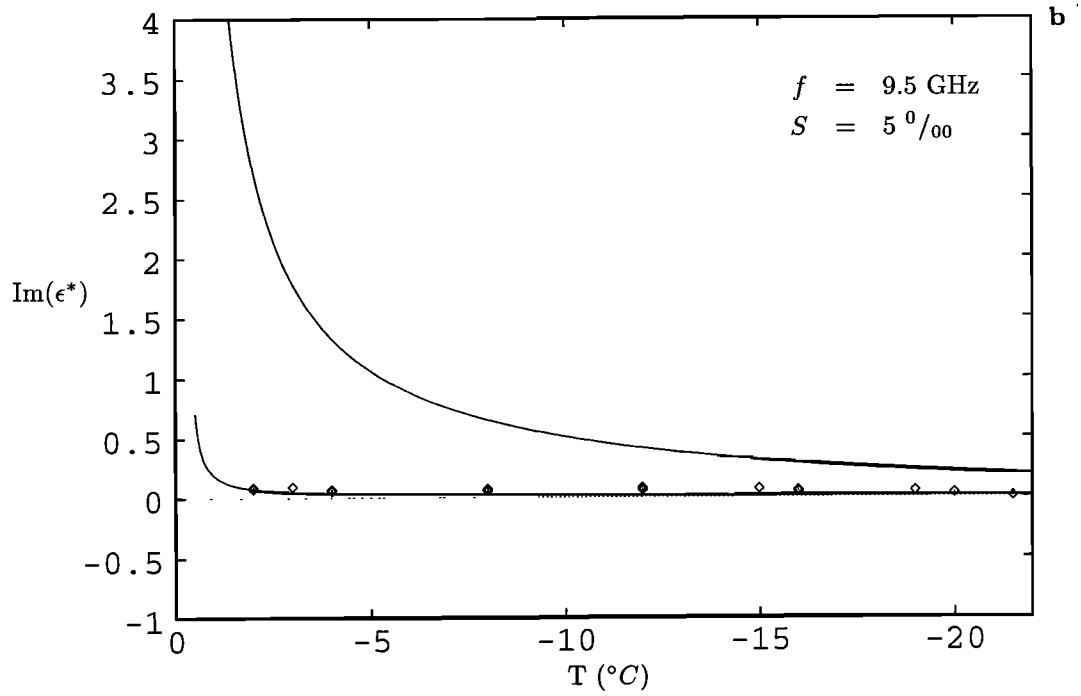

Figure 6b. Comparison of experimental data on ϵ^* with upper and lower bounds on $Im(\epsilon^*)$ obtained from R_2, as a function of temperature. at 9.5 GHz.

apply the Golden–Milton bounds to three–component sea ice.

Appendix: The Analytic Continuation Method

Here we describe in more detail following *Golden* [1986], how the bounds R_0, R_1, and R_2 are obtained. We begin with the fundamental representation formula presented in section 2,

$$F(s) = \int_0^1 \frac{d\mu(z)}{s - z}, \qquad \text{(A1)}$$

where

$$F = 1 - \epsilon^*/\epsilon_2, \quad s = 1/(1 - \epsilon_1/\epsilon_2), \qquad \text{(A2)}$$

and μ is a positive measure on [0,1]. An alternative operator representation for $F(s)$ can be obtained from manipulation of (2)–(5),

$$F(s) = < \chi_1[(s + \Gamma\chi_1)^{-1}\mathbf{e}_k] \cdot \mathbf{e}_k >, \qquad \text{(A3)}$$

where $\Gamma = \nabla(-\Delta)^{-1}\nabla\cdot$. In the Hilbert space $L^2(\Omega)$ with χ_1 in the inner product, $\Gamma\chi_1$ is a bounded self–adjoint operator of norm less than or equal to one. The integral representation (A1) is the spectral representation of the resolvent $(s+\Gamma\chi_1)^{-1}$, where μ is the spectral measure of the family of projections of $\Gamma\chi_1$, which provides a proof of (A1). We then see explicitly how μ depends on the geometry through χ_1. Another proof of (A1) exploits the Herglotz property of $F(s)$.

Now we describe how (A3) can be used to inject geometrical information into the measure μ. First, for $|s| > 1$, (A1) can be expanded about a homogeneous medium ($s = \infty$ or $h = 1$),

$$F(s) = \frac{\mu_0}{s} + \frac{\mu_1}{s^2} + \ldots, \quad \mu_n = \int_0^1 z^n d\mu(z). \qquad \text{(A4)}$$

This is equivalent to a Taylor series expansion of $m(h) = \epsilon^*/\epsilon_2(\epsilon_1/\epsilon_2)$ around $h = 1$. Equating (A4) to the same expansion of (A3) yields

$$\mu_n = (-1)^n < \chi_1[(\Gamma\chi_1)^n\mathbf{e}_k] \cdot \mathbf{e}_k > . \qquad \text{(A5)}$$

It is through this moment formula that correlation information about the geometry is injected into the integral representation. If all the moments μ_n are known, then the measure μ is uniquely determined. Then (A1) provides the analytic continuation of the power series in (A4) to its full domain of analyticity, which is the full complex s plane excluding [0,1].

Bounds on ϵ^* are obtained from (A1) as follows. First we describe how R_0 is obtained. By (A5), μ_0 equals p_1, the volume fraction of medium 1. Then

$$0 \le \mu_0 \le 1. \qquad \text{(A6)}$$

For $s \in \mathbb{C}\backslash[0,1]$, where $\mathbb{C}$ is the complex plane, $F(s,\mu)$ in (A1) is a linear functional from the set M of positive measures of mass ≤ 1 on [0,1] into $\mathbb{C}$. Now M is a compact, convex set of measures. The extreme points (or boundary) of the range of values of $F(s,\mu)$ in $\mathbb{C}$ are attained by one–point (Dirac) measures $\alpha\delta_a, 0 \le \alpha \le$

$1, 0 \le a \le 1$, since they are the extreme points of M. For these measures (which are so-called "δ functions"), F has the form

$$F(s) = \frac{\alpha}{s - a}, \quad 0 \le \alpha \le 1, \quad 0 \le a \le 1. \tag{A7}$$

The condition $F(s = 1) \le 1$ determines the allowed region R_0 in the F plane. It is the image of the triangle in (α, a) space, defined by $\alpha + a \le 1, 0 \le \alpha \le 1, 0 \le a \le 1$, under the mapping (A7), which is described in (15). The bounds in (15) are optimal and can be attained by laminates of ϵ_1 and ϵ_2 aligned perpendicular and parallel to the applied field. The arcs are traced out as the volume fraction varies.

If the volume fractions p_1 and $p_2 = 1 - p_1$ are fixed as well as s, then μ_0 is fixed, with

$$\mu_0 = p_1. \tag{A8}$$

Then applying a similar extremal analysis as above shows that the values of F lie inside the circle parametrized by

$$C_1(z) = \frac{p_1}{s - z}, \quad -\infty \le z \le \infty. \tag{A9}$$

On the other hand,

$$E(s) = 1 - \epsilon_1/\epsilon^* = \frac{1 - sF(s)}{s[1 - F(s)]} \tag{A10}$$

is also a Herglotz function like $F(s)$ and has a representation

$$E(s) = \int_0^1 \frac{d\nu(z)}{s - z}. \tag{A11}$$

Expansion of $E(s)$ yields $\nu_0 = p_2$, so that the values of E lie inside the circle

$$\hat{C}_1(z) = \frac{p_2}{s - z}, \quad -\infty \le z \le \infty. \tag{A12}$$

In the ϵ^* plane the intersection R_1 of these two regions is bounded by two circular arcs corresponding to $0 \le z \le p_2$ in (A9) and $0 \le z \le p_1$ in (A12). These bounds are optimal and can be attained by a composite of uniformly aligned spheroids of material 1 in all sizes coated with confocal shells of material 2, and vice versa. These arcs are traced out as the aspect ratio varies.

If the material is further assumed to be statistically isotropic, then

$$\mu_1 = \frac{p_1 p_2}{d}, \tag{A13}$$

so that in view of (A4), F is known to second order,

$$F(s) = \frac{p_1}{s} + \frac{p_1 p_2/d}{s^2} + \dots . \tag{A14}$$

A convenient way of including this information is to use the transformation of *Bergman* [1982],

$$F_1(s) = \frac{1}{p_1} - \frac{1}{sF(s)}. \tag{A15}$$

The function $F_1(s)$ is, again, a Herglotz function which has the representation

$$F_1(s) = \int_0^1 \frac{d\mu^1(z)}{s - z}. \tag{A16}$$

Under (A14), F_1 is known only to first order

$$F_1(s) = \frac{p_2/p_1 d}{s} + \dots , \tag{A17}$$

which forces the zeroth moment μ_0^1 of μ^1 to be

$$\mu_0^1 = p_2/p_1 d. \tag{A18}$$

Then applying the same procedure as for R_1 yields the bound R_2, where the boundaries are circular arcs parameterized by (25) and (26). We remark that higher-order correlation information can be conveniently incorporated by iterating (A15), as done by *Golden* [1986].

Acknowledgments. The author would like to thank Eric Bair for preparing the graphs and for helpful suggestions in comparing the bounds with the data. In addition, the author is grateful to Steve Ackley, Steve Arcone, Tony Gow, Vicky Lytle, Jin Kong, and Graeme Milton for helpful discussions on sea ice and general dielectric theory. Finally, the author expresses his thanks to Art Jordan and Reza Malek-Madani at ONR for their encouragement and support of this work. This research was supported by ONR Grant N000149310141 and NSF Grant DMS-93073244.

References

Addison, J., Electrical properties of saline ice, *J. Appl. Phys.*, *40*, 3105–3114, 1969.

Arcone, S. A., A. J. Gow, and S. McGrew, Structure and dielectric properties at 4.8 and 9.5 GHz of saline ice, *J. Geophys. Res.*, *91*, 14,281–14,303, 1986.

Bergman, D. J., The dielectric constant of a composite material–A problem in classical physics, *Phys. Rep. C*, *43*, 377–407, 1978.

Bergman, D. J., Exactly solvable microscopic geometries and rigorous bounds for the complex dielectric constant of a two-component composite material, *Phys. Rev. Lett.*, *44*, 1285, 1980.

Bergman, D. J., Rigorous bounds for the complex dielectric constant of a two–component composite, *Ann. Phys.*, *138*, 78, 1982.

Berlyand, L., and K. Golden, Exact result for the effective conductivity of a continuum percolation model, *Phys. Rev. B, Condensed Matter*, *50*, 2114–2117, 1994.

Bruno, O., The effective conductivity of strongly heterogeneous composites, *Proc. R. Soc. London A*, *433*, 353–381, 1991.

Cherepanov, N. V., Spatial arrangement of sea ice

crystyal structure, *Probl. Arkt. Antark.*, *38*, 137–140, 1971.

Frankenstein, G., and R. Garner, Equations for determining the brine volume of sea ice from −0.5° to −22.9° C, *J. Glaciol.*, *6*, 943–944, 1967.

Golden, K., Bounds on the complex permittivity of a multicomponent material, *J. Mech. Phys. Solids*, *34*, 333–358, 1986.

Golden, K., Convexity and exponent inequalities for conduction near percolation, *Phys. Rev. Lett.*, *65*, 2923–2926, 1990.

Golden, K., Exponent inequalities for the bulk conductivity of a hierarchical model, *Commun. Math. Phys*, *43*, 467–499, 1992.

Golden, K., Scaling law for conduction in partially connected systems, *Proceedings of ETOPIM '93, Physica A.*, *207*, 213–218, 1994.

Golden, K. M., and S. F. Ackley, Modeling of anisotropic electromagnetic reflection from sea ice, *J. Geophys. Res.*, *86*, 8107–8116, 1981.

Golden, K., and G. Papanicolaou, Bounds for effective parameters of heterogeneous media by analytic continuation, *Comm. Math. Phys.*, *90*, 473–491, 1983.

Golden, K., and G. Papanicolaou, Bounds for effective parameters of multicomponent media by analytic continuation, *J. Stat. Phys.*, *40*, 655–667, 1985.

Hashin, Z., and S. Shtrikman, A variational approach to the theory of effective magnetic permeability of multiphase materials, *J. Appl. Phys.*, *33*, 3125–3131, 1962.

Hoekstra, P., and P. Capillino, Dielectric properties of sea and sodium chloride ice at UHF and microwave frequencies, *J. Geophys. Res.*, *76*, 4922–4931, 1971.

Kovacs, A., and R. M. Morey, Radar anisotropy of sea ice due to preferred azimuthal orientation of the horizontal c-axis of ice crystals, *J. Geophys. Res.*, *83*, 6037–6046, 1978.

Kozlov, S. M., Geometric aspects of homogenization, *Russ. Math. Surv.*, *44*, 91, 1989.

Mätzler, C., and U. Wegmüller, Dielectric properties of fresh–water ice at microwave frequencies, *J. Phys. D Appl. Phys.*, *20*, 1623–1630, 1987.

Milton, G. W., Theoretical studies of the transport properties of inhomogeneous media, Technical Report Physics IV, Dept. of Theor. Phys., Univ. of Sydney, 1979.

Milton, G. W., Bounds on the complex permittivity of a two-component composite material, *J. Appl. Phys.*, *52*, 5286–5293, 1981.

Milton, G. W., Multicomponent composites, electrical networks and new types of continued fractions I, *Comm. Math. Phys.*, *111*, 281–327, 1987a.

Milton, G. W., Multicomponent composites, electrical networks and new types of continued fractions II, *Comm. Math. Phys.*, *111*, 329–372, 1987b.

Milton, G. W., and K. Golden, Thermal conduction in composites, in *Thermal Conductivity 18*, edited by T. Ashworth and D. R. Smith, pp. 571–582, Plenum Press, New York, 1985.

Sihvola, A. H., and J. A. Kong, Effective permittivity of dielectric mixtures, *IEEE Trans. Geosci. Remote Sensing*, *26*, 420–429, 1988.

Stogryn, A., An analysis of the tensor dielectric constant of sea ice at microwave frquencies, *IEEE Trans. Geosci. Remote Sensing*, *GE-25*, 147–158, 1985.

Stogryn, A., and G. J. Desargant, The dielectric properties of brine in sea ice at microwave frequencies, *IEEE Trans. Antennas Propag.*, *AP-33*, 523–532, 1985.

Tinga, W. R., A. G. Voss, and D. F. Blossey, Generalized approach to multiphase dielectric mixture theory, *J. Appl. Phys.*, *44*, 3897–3902, 1973.

Vant, M. R., R. O. Ramseier, and V. Makios, The complex-dielectric constant of sea ice at frequencies in the range 0.1–40 GHz, *J. Appl. Phys.*, *49*, 1264–1280, 1978.

Weeks, W. F., and S. F. Ackley, The growth, structure and properties of sea ice, *Cold Reg. Res. and Eng. Lab. Monogr. 82-1*, pp. 130, 1982.

Weeks, W. F., and A. J. Gow, Crystal alignments in the fast ice of Arctic Alaska, *J. Geophys. Res.*, *85*, 1137–1146, 1980.

K. Golden, Department of Mathematics, University of Utah, Salt Lake City, UT 84112.

(Received September 2, 1993; revised June 17, 1994; accepted November 14, 1994.)